How the Oblique Drift Instability Alters Solar Wind Heating and Constrains the Distribution of Solar Wind Observations

Mihailo M. Martinović[*] and Kristopher G. Klein
Lunar and Planetary Laboratory, University of Arizona, Tucson, Arizona 85721, USA

Leon Ofman[†]
The Catholic University of America, Washington, DC 20064, USA
and Heliophysics Science Division, NASA Goddard Space Flight Center, Greenbelt, Maryland 20771, USA

Yogesh and Gregory G. Howes
Department of Physics and Astronomy, University of Iowa, Iowa City, Iowa 52242, USA

Jaye L. Verniero
Heliophysics Science Division, NASA, Goddard Space Flight Center, Greenbelt, Maryland 20771, USA

Peter H. Yoon
Institute for Physical Science and Technology, University of Maryland, College Park, Maryland 20742-2431, USA

Daniel Verscharen
Mullard Space Science Laboratory, University College London, Dorking, RH5 6NT, United Kingdom

Benjamin L. Alterman
Heliophysics Science Division, NASA, Goddard Space Flight Center, Greenbelt, Maryland 20771, USA

(Received 18 February 2026; accepted 21 May 2026; published 24 June 2026)

Ion-driven plasma instability thresholds, derived from linear theory, constrain the distribution of solar observations in parameter space, defining boundaries of stable plasma parameters. Excursions beyond these thresholds result in the emission of energy, transferred from particles to coherent electromagnetic waves, acting to adjust the system toward a more stable configuration. In this Letter, we use linear Vlasov-Maxwell theory to define parametric limits for a low-β plasma that contains a drifting proton beam or helium (α-particle) population. A sufficiently fast and dense drifting population triggers an oblique drift instability (ODI). This instability decreases the velocity drift between the thermal core proton and secondary populations and prevents the ratio of core thermal to magnetic pressure β_c from decreasing below a minimum value by increasing the temperatures—i.e., heating—of both the core and drifting populations. Our theoretical results are of interest for Parker Solar Probe observations, as they provide an additional mechanism for perpendicular heating of ions active in the sub-Alfvénic solar wind. The ODI may explain the discrepancy between long-standing expectations of measurements of very low-β plasmas with very large ion temperature anisotropies in the near-Sun environment and *in situ* observations, where β is consistently measured above a few percentages and the secondary ion populations drift faster than the bulk of the proton population by no more than approximately the local Alfvén speed.

DOI: 10.1103/nlq9-2g37

Introduction—Many astrophysical plasmas, including the solar wind in the inner heliosphere, are weakly collisional, allowing departure from the local thermodynamic equilibrium (LTE). Characterizing the thermodynamics of weakly collisional plasmas is a long-standing open question, whose answer is central to explaining the heating and acceleration of the solar wind [1,2]. For decades, surveys of *in situ* solar wind proton observations have been routinely represented with the so-called "Brazil" plot—a phase space determined by $\beta_{\parallel,p}$—thermal to the magnetic pressure ratio of protons—and temperature anisotropy $T_{\perp,p}/T_{\parallel,p}$, with $\perp$ and $\parallel$ defined with respect to the background magnetic field vector **B** (Fig. 1). The "Brazil" plot demonstrates that the solar wind evolution is limited by instabilities [3], where in high-β wind, usually further away from the Sun, even the smallest changes in anisotropy can cause the thermal-pressure-dominated plasma to become intensely unstable [4].

[*]Contact author: mmartinovic@arizona.edu
[†]Tel Aviv University, Tel Aviv, Israel.

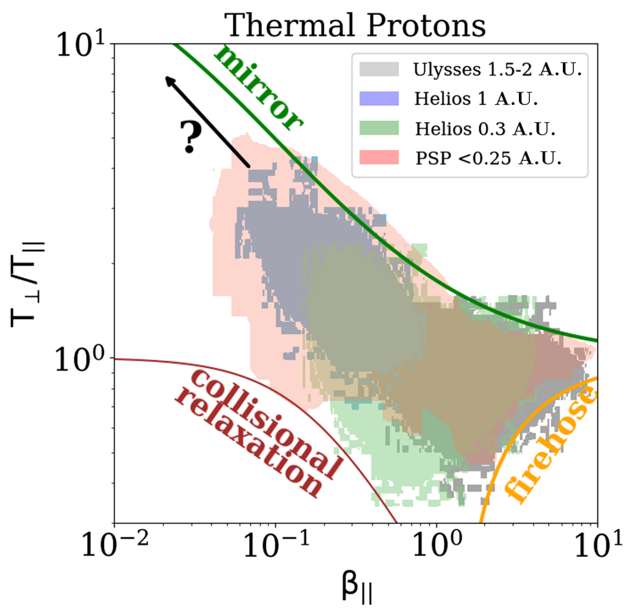

FIG. 1. Summary of proton measurements of previous missions. The three sides of the plot limit the "allowed" parameter space, while the plasma moving to a lower β state does not have obvious limitations in linear theory of a single population. Owing to the limited proton core and beam modeling for included missions, we use single component fits and the associated instability thresholds.

The data are remarkably well constrained by the parametric theoretical thresholds [5,6] of the Alfvén ion-cyclotron (AIC) and mirror instabilities for $T_{\perp,p}/T_{\parallel,p} > 1$ and the oblique and parallel firehose instabilities for $T_{\perp,p}/T_{\parallel,p} < 1$ [2,7]. The low-β region is constrained by collisional relaxation expected for propagation times at 1 A.U. as estimated by quasilinear theory [8] for $T_{\perp,p}/T_{\parallel,p} < 1$. On the contrary, it has an "open-ended" part for $T_{\perp,p}/T_{\parallel,p} > 1$, where even strongly anisotropic plasma can remain linearly stable. Linear theory for a single ion component does not provide any limit on how low plasma $\beta_{\parallel,p}$ can be. However, for $T_{\perp,p}/T_{\parallel,p} > 1$, the observations of $\beta_{\parallel,p} < 0.1$ are relatively rare beyond 0.3 A.U. [9,10]. Owing to the lack of *in situ* observations, low-β instability thresholds for inner heliospheric conditions have received some attention [8,11], but have not been investigated as rigorously as those with $\beta \sim 1$. We propose an instability mechanism driven by relative drifts between ion populations that limits the solar wind from filling the low-β, high $T_{\perp,p}/T_{\parallel,p}$ region of parameter space.

Launched in 2018, the Parker Solar Probe (PSP) [12] has reached the so-called Alfvén surface [13], inside which the solar wind bulk speed is lower than the Alfvén speed $v_A = w_{\parallel,p}/\beta_{\parallel,p}^{1/2} = B/\sqrt{\mu_0 m_p n_p}$, where $w_{\parallel,p}^2 = 2k_B T_{\parallel,p}/m_p$ is the proton thermal speed and m_p is the mass of the proton. We define the parallel proton plasma beta $\beta_{\parallel,p} = 2\mu_0 n_p k_B T_{\parallel,p}/B^2$ and temperature anisotropy $T_{\perp,p}/T_{\parallel,p}$; μ_0, k_B, and n_p are the magnetic permeability of vacuum, Boltzmann constant, and proton density, respectively. At distances within the Alfven surface, Alfvén waves generated *in situ* can travel back to the surface of the Sun. It has been hypothesized that inside this surface the solar wind heating is significantly enhanced [14,15]. Various mechanisms have been invoked to explain preferential perpendicular heating in this region, e.g., stochastic heating [16,17] or IC heating [18–20]. Initial *in situ* measurements in a sub-Alfvénic plasma [21,22] have not consistently shown the enhancement of these processes in the near-Sun solar wind at or below the Alfvén surface.

Each component of the plasma velocity distribution function (VDF) can be anisotropic, with distinct temperatures perpendicular and parallel to the direction of the magnetic field [23]. The two populations can also have different speeds along the magnetic field, producing a commonly observed intercomponent drift [24]. These anisotropies and relative drifts often store a significant percentage of the system's "free" energy [25–27]. Significant departures from LTE can drive the system unstable, generating electromagnetic fluctuations that act to reduce the free energy source of the instability [28,29]. The predictions made by the linear Vlasov-Maxwell theory imply that the onset of instabilities at kinetic scales effectively constrains the nonthermal features of the VDF and, consequently, the parameter space distribution [23,30–35].

We hypothesize that this low-β limit is evidence that an oblique drift instability (ODI) is converting free energy carried by the relative drift between α particles and/or a proton beam (with respect to the proton core) into both perpendicular and parallel thermal energy. This heating does not require the interaction of particles with the background turbulence, or with existing coherent waves. The process is driven by the same type of wave-particle resonance and only slightly quantitatively different when driven by drifting protons or α particles. We find that the ODI is important for both limiting the low-β values by heating the protons and for constraining Δv_α to be consistently below the local Alfvén speed [36].

Oblique electromagnetic ion beam instabilities have been studied extensively in the context of proton beams and temperature anisotropy driven instabilities (e.g., Refs. [29,37,38]) including their behavior in expanding box simulations [39]. These studies established that the fastest growing modes often occur at oblique angles and can lead to beam relaxation and wave generation. However, the role of ODI in low-β solar wind conditions, particularly in the presence of α-particle drifts, resonant ion heating, and nonlinear evolution into secondary instabilities, has not been systematically investigated. In this Letter, we demonstrate, for the first time, that the ODI operates as an efficient mechanism for converting drift energy into ion heating and acts as a regulator of ion drift speeds in the solar wind.

Linear theory of the low-β ODI—Assuming a combination of relatively drifting bi-Maxwellian VDFs, the solution to the wave equation $|\underline{\mathbf{D}}(\omega, \mathbf{k}, \mathcal{P})| = 0$ for a hot, magnetized plasma allows an estimate of the complex frequency at maximum wave growth rate $\omega = \omega_r + i\gamma_{\max}$ associated with wave vector $\mathbf{k}$ and plasma parameters $\mathcal{P}$, the power emitted for each component over the course of a single wave period P_j, electric $\delta\mathbf{E}$ and magnetic $\delta\mathbf{B}$ field fluctuations and polarizations for the most unstable mode (MUM). Here, we use the PLUME and PLUMAGE solvers when a bi-Maxwellian VDF shape is assumed [40–42] and ALPS solver [43,44] to analyze the modes driven by non-Maxwellian VDFs obtained from simulations (more details in the Supplemental Material [45], which contains Refs. [50–53]).

Figure 2 shows the PLUMAGE analysis of a core proton and drifting α-particle component for a set of 625 logarithmically spaced $\beta_{\|,p}$–$T_{\perp,p}/T_{\|,p}$ pairs of values with all the plasma parameters $\mathcal{P}$ (n_α/n_p, $\Delta v_\alpha/v_A$, $T_{\perp,p,\alpha}/T_{\|,p,\alpha}$) fixed, colored by the MUM angle of propagation $\theta_{\mathbf{kB}}$. We set $T_{p,\perp}/T_{p,\|} = 3$, and $T_{\perp,\alpha}/T_{\|,\alpha} = T_{\|,\alpha}/T_{\|,p} = 1$ to focus on the drift as the main source of free energy. An oblique drift-induced mode will become unstable at low β with both $\gamma_{\max}/\Omega_p$—increasing with the dot size—and the angle of propagation $\theta_{\mathbf{kB}}$ increasing as $\beta_{\|,p}$ decreases. We note the existence of an "island" of stability for $\Delta v_\alpha/v_A < 0.9$, $\beta_{\|,p} \in [0.005, 0.02]$, and $T_{\perp,p}/T_{\|,p} \lesssim 5$—conditions common for near-Sun solar wind [36].

We further investigate a slice of constant proton anisotropy, denoted with a *black rectangle* in Fig. 2, using PLUME to identify nine solutions: α cyclotron, Alfvén, fast magnetosonic, and slow magnetosonic waves—all four having both distinct forward and backward propagating solutions in the plasma frame due to velocity space symmetry breaking associated with the drifting components, and a nonpropagating entropy mode. In Fig. 3 *black dots* illustrate the PLUMAGE inferred MUM growth rate and PLUME inferred emitted (absorbed) power solutions for both parallel AIC and oblique ODI, both of which originate from the same forward propagating Alfvén mode. For drifts lower than the Alfvén speed, we see the range of $\beta_{\|,p}$ values for which the plasma is stable, with lower- and higher-β cases dominated by the oblique and parallel unstable modes, respectively. If the drift is increased to $\Delta v_\alpha/v_A = 1$, both modes can be active in the same interval, implying that the oblique waves can still extract energy from the α component while the intensively growing parallel AIC mode is active, as will be demonstrated in nonlinear hybrid simulations.

For a closer examination of the ODI, we show its emitted power as a function of $\Delta v_\alpha/v_A$. Crucially, the instability threshold for the ODI requires smaller α-particle drifts to overcome the proton emission as $\beta_\|$ decreases. Plasmas with $\beta_\| < 1\%$ have a maximum stable value of $\Delta v_\alpha/v_A$ below 0.85, implying that this type of resonant instability will become active prior to any firehoselike instability where excess parallel pressure is the main free energy source [25]. The mode properties and the maximum drifts are preserved for low α-particle densities and only marginally vary with n_α/n_p, while not varying with proton parameters (not shown).

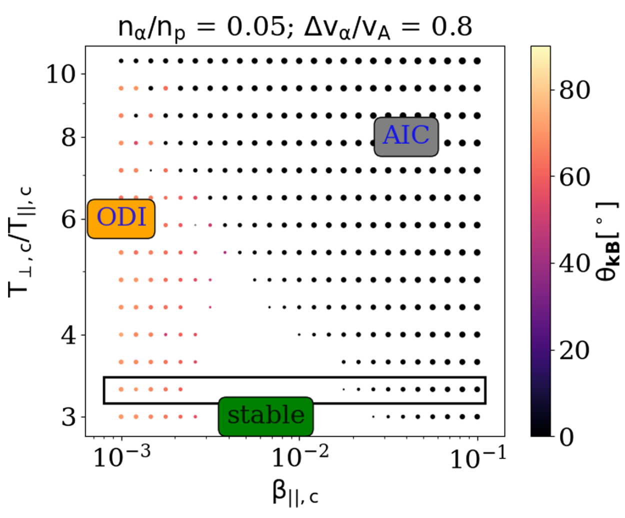

FIG. 2. The "island" of stability between the forward Alfvén mode unstable in the direction parallel to $\mathbf{B}$—the proton AIC instability—and the ODI at lower proton core β_c for fixed n_α and Δv_α The size of the points increases logarithmically with the MUM growth rate $\lg(\gamma_{\max}/\Omega_p)$, covering the range between 10^{-3} and 0.3.

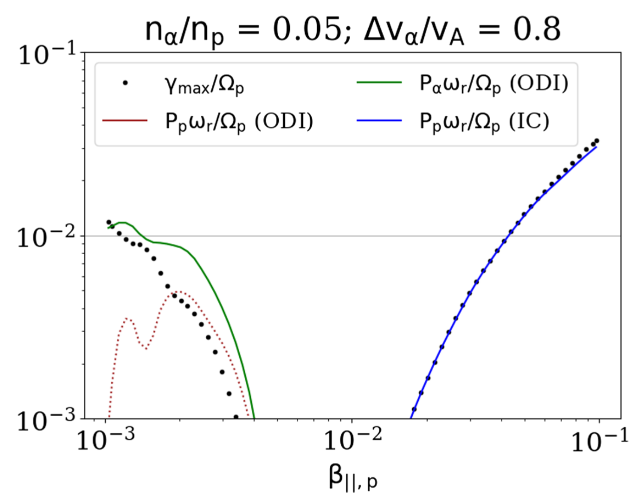

FIG. 3. Overview of the ion contributions to the AIC and ODI instabilities for intervals marked with a black rectangle ($T_{\perp,c}/T_{\|,c} \approx 3.25$) in Fig. 2, with solid (dashed) lines indicating power emission (absorption). Both instabilities emit a forward-propagating Alfvén mode. The PLUMAGE growth rate and PLUME power transmission solutions are marked with dots and lines, respectively. Note that in the linear approximation $\sum_j P_j \approx \gamma/\omega_r$ [28].

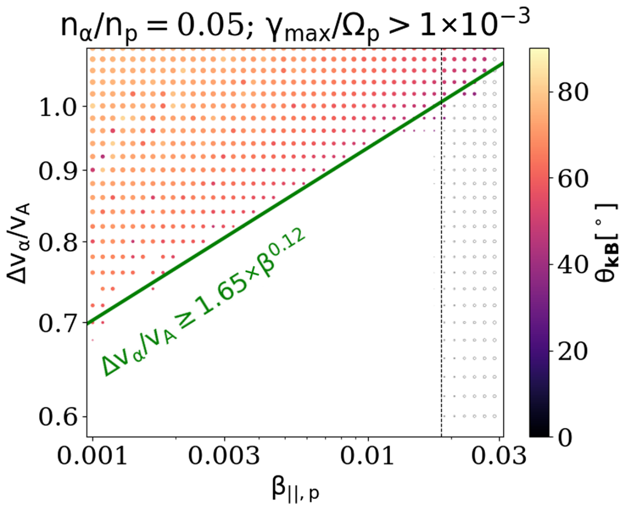

FIG. 4. ODI mode growth rates and propagation angle (as in Fig. 2) dependence on the velocity drift. The best-fit parametric instability threshold is shown in green.

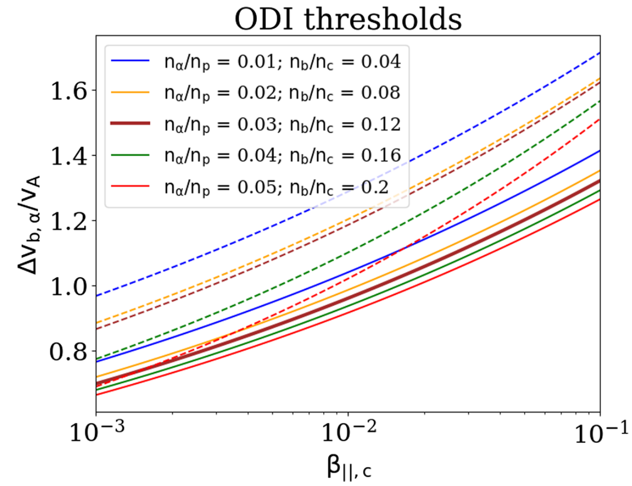

FIG. 5. ODI instability thresholds for varying α-particle densities (*solid lines*) for $\gamma/\Omega_p = 10^{-3}$. *Dashed lines* provide comparison given by [29] for the proton-beam induced ODI with beam densities n_b with the same mass flux as the α cases.

Figure 4 illustrates that the ODI instability threshold in logarithmic space very nearly follows a straight line. This feature holds at least up to $n_\alpha/n_p \lesssim 10\%$ and for growth rates ranging from $\gamma_{\max}/\Omega_p \in (10^{-4}, 2\times10^{-2})$. This trend enables a linear fit of $\Delta v_\alpha/v_A = \hat{m}\log_{10}(\beta_{\|,p}) + \hat{b}$ to obtain the numerical expression for the threshold, with the example labeled along the fitted *green* line. We repeat the fitting procedure for various density ratios. Fitting slopes and intercepts for different n_α/n_p while keeping the growth rate fixed enables another stage of linear fits with relative density as the independent variable. These results can be combined to obtain the instability condition for any onset growth rate. For $\gamma_{\max}/\Omega_p = 10^{-3}$ we get

$$\Delta v_\alpha/v_A \geq 10^{0.255-0.4n_\alpha/n_p}\beta_{\|,p}^{0.116-0.38n_\alpha/n_p}. \quad (1)$$

This analytical representation accurately describes the α-particle-induced ODI growth rates shown in Fig. 5.

We directly compare this instability to the one described in Sec. 8.5 of [29], where the proton beam drives the ODI with the drift being the primary source of free energy. We expand on the results of [29] to normalize relative proton beam density in such a way that the mass flux of *proton* beams and α particles remains equal, showing them in the same color on Fig. 5. The drift value required for α particles to drive the instability is consistently below the one for proton beams over a wide range of β values due to the difference in resonance conditions for the underlying $n = -1$ resonance (see next section). As the proton beams are not consistently present in the solar wind [54–56], α particles remain the primary driver of the ODI and regulator of the low-β limit in the solar wind.

Plasma β limits in hybrid simulations—To illustrate the transfer of energy from drifting α particles to thermal protons via the ODI, we use a well-established 2.5D hybrid-PIC code that captures ion dynamics across multiple ion-cyclotron periods with realistic proton mass and Alfvén-to-light speed ratio, bypassing standard particle-in-cell (PIC) code limitations by representing electrons as a massless neutralizing fluid [57–59]. Our setup is similar to recent studies [60–62]—we use a 256^2 spatial grid with 512 particles per cell, fully sufficient to capture plasma dispersion at ion scales. Full details for the simulation can be found in the Appendix of the Supplemental Material [45], which includes Refs. [63–70].

The top panels of Fig. 6 show the initial state of the simulation. The α particles of density $n_\alpha/n_p = 5\%$ drift at

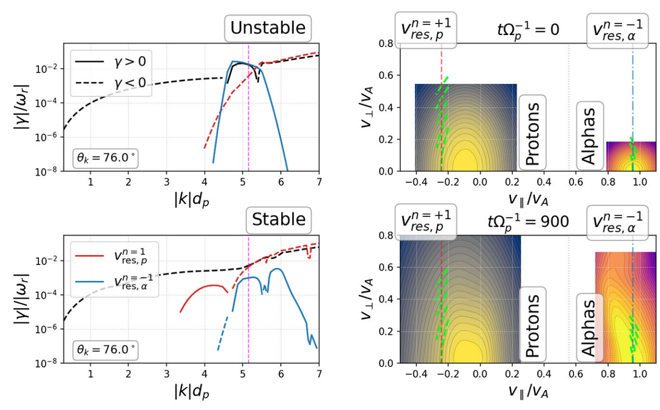

FIG. 6. Growth (solid lines, left column) and damping rates (dashed) for proton and α VDFs representative of the young solar wind unstable to the ODI at early (top right) and late (bottom right) times in the simulation. The emitting α particle ($n = -1$) and absorbing proton ($n = 1$) cyclotron resonances for the most unstable mode are marked by blue and red lines. Particles are scattered along resonance curves (green) for the highlighted wave vector (magenta, left column), leading to wave emission and heating.

$\Delta v_\alpha / v_A = 0.95$ with respect to protons, driving the ODI for the low $\beta_{\parallel,p} = 0.003$ conditions. The initial values of $T_{p,\perp}/T_{p,\parallel} = 3$ and $T_{\alpha,\perp}/T_{\alpha,\parallel} = 1$ are stable with respect to AIC. We note that as the ODI is driven by the particle drift, the instability onset is very weakly dependent on $T_{\alpha,\perp}/T_{\alpha,\parallel}$. The ODI is induced by the drift of secondary populations—proton beams and α particles—with the wave vector of the unstable mode at an oblique angle with respect to the background magnetic field $\mathbf{B}_0$; dispersion relations are plotted as a function of $|k|d_p$ for clarity. The ODI couples via cyclotron resonances, where the relation of the resonant particle velocity $\mathbf{v_{res}}$ (*green dashed* lines), real frequency ω_r, and wave number $\mathbf{k}$ is given as $\omega_r - k \cdot \mathbf{v_{res}} - n\Omega_s = 0$, where Ω_s is the cyclotron frequency for species s and n is an integer. At wavelengths a fraction of the inertial length, but notably larger than the gyroradius due to low β values, the $n = -1$ cyclotron resonance (*blue* line) emits an unstable mode, scattering initially isotropic α particles along the *green* resonance curves in the velocity space. These linear dispersion relations are calculated directly from the simulated VDFs using ALPS [43,44]; see the Supplemental Material [45] for more details. The emitting wave vectors are shown by *solid* lines in the left panels, while non-negligible damping is marked by *dashed* lines, showing notable absorption by protons through the $n = 1$ resonance, marked in *red*. In both cases, the α particles have a range of wave vectors where the power is emitted, but is then either partially or entirely absorbed by the protons. For the system to be considered unstable at given $\mathbf{k}$, the total emission at that $\mathbf{k}$ must be larger than the absorption.

During later stages of the simulation (bottom panels in Fig. 6), some of the free energy from the α-particle drift is drained, decreasing $\Delta v_\alpha / v_A$, but increasing $T_{\perp,\alpha}$, $T_{\perp,p}$, and $T_{\parallel,p}$ in the process. This final state is stable with respect to ODI, as the emission of α particles does not surpass the absorption of the protons (bottom left), but the transfer of energy from one component to another is still active, and the protons continue to be heated via $n = -1$ α-particle resonance (magenta line).

This implies a prolonged process that will remain active until the free energy from the velocity drift is drained, heating both the proton and α-particle distributions in both parallel and perpendicular directions. The increase in $T_{p,\perp}$ leads to a secondary intense forward propagating AIC parallel propagating instability, depositing some of the drift free energy into coherent plasma waves. The fraction of energy deposited in the parallel direction increases $T_{p,\parallel}$ and thus $\beta_{p,\parallel}$. This process is more intensive for lower $\beta_{p,\parallel}$, hence putting a limit to its minimum value.

Discussion and conclusions—The AIC and mirror instability provide a threshold for the maximum value of proton anisotropy in the solar wind at $\beta \gtrsim 1$ [5,30]. While there are quasilinear models that hypothesize the low-β, $T_{\perp,p}/T_{\parallel,p} < 1$ region is regulated by collisions [8,11], the low-β, $T_{\perp,p}/T_{\parallel,p} > 1$ region has no solid theoretical or observational constraints. However, the measurements obtained from *PSP* encounters (perihelia) shows higher lower-bound values of β compared to prelaunch predictions [71].

We propose a previously established instability mechanism—the oblique drift instability—to provide a novel explanation of the lower limit on the observations of $\beta_{\parallel,p}$, the magnitudes of α-particle drifts with respect to the protons, which are also very rarely observed to be faster than a single Alfvén velocity [36,72], as well as the heating of both the protons and alphas. The presence of drifting α particles leads to the emission of power for oblique wavemodes via the $n = -1$ cyclotron resonance. If $\beta_{\parallel,p}$ is sufficiently large, the increased width of the proton VDF fills the velocity space with enough particles that can absorb this emitted power, creating a stable configuration. In contrast, lowering the value of $\beta_{\parallel,p}$ decreases the proton phase space density at the appropriate resonant velocities, enabling the α-driven emission to destabilize the equilibrium. The emitted power from the alphas is then absorbed by thermal protons through the $n = 1$ cyclotron resonance, leading to proton heating and increasing $\beta_{\parallel,p}$. This setup effectively restricts the lowest values of $\beta_{\parallel,p}$ "allowed" by the linear theory. It also provides a constant mechanism to both limit the secondary population drift and to heat thermal protons and secondary populations.

As the set of VDF parameters specific for ODI corresponds to the ones observed in the sub-Alfvénic solar wind, the ODI may serve as an additional avenue of intense solar wind heating in this region of the inner heliosphere. Just outside of the corona ($r \sim 2R_\odot$) the role of ODI is unclear. Although Alfvén speed is very high compared to the thermal speed, it is not currently understood how the α particle and proton beam drifts evolve once the collisions are no longer dominant. At larger radial distances plasma β becomes too high for the ODI to be significant, leaving the sub-Alfvénic wind as a specific region where this mechanism can become very intense and act as the primary regulator of solar wind evolution via a heating mechanism not previously considered in models.

This result will be further tested with *PSP* solar encounter observations as statistically significant amounts of observations in low-β solar wind are being collected by the spacecraft. The caveats of the observational work will be addressed in future work, as the data products of the mission mature and are able to confidently separate multiple proton components as well as a potential α-particle beam [72,73]. Finally, since the instability thresholds can be very steep in velocity space, the future work requires careful treatment of instrument uncertainties when comparing measured VDFs with our predictions.

Acknowledgments—M. M. M. and K. G. K. were financially supported by NASA Grants No. 80NSSC22K1011, No. 80NSSC19K1390, No. 80NSSC23K0693, No. 80NSSC19K0829, and No. 80NSSC24K0724. L. O. and Y. acknowledge support by NASA Grant No. 80NSSC24K0724 and NSF SHINE Grant No. AGS-2300961. Y. acknowledges the support by the College of Liberal Arts and Sciences at the University of Iowa. D. V. is supported by STFC Consolidated Grant No. ST/W001004/1. B. L. A. is supported by NASA Grant No. 80NSSC22K1011. The authors would also like to thank members of ISSI International Team No. 563 supported by the International Space Science Institute (ISSI) in Bern for productive conversations regarding this work. An allocation of computer time from the UA Research Computing High Performance Computing at the University of Arizona is gratefully acknowledged.

Data availability—The data are not publicly available. The data are available from the authors upon reasonable request.

[1] E. Marsch, Helios: Evolution of distribution functions 0.3–1 A.U., Space Sci. Rev. **172**, 23 (2012).

[2] D. Verscharen, K. G. Klein, and B. A. Maruca, The multi-scale nature of the solar wind, Living Rev. Solar Phys. **16**, 5 (2019).

[3] L. Matteini, P. Hellinger, B. E. Goldstein, S. Landi, M. Velli, and M. Neugebauer, Signatures of kinetic instabilities in the solar wind, J. Geophys. Res. Space Phys. **118**, 2771 (2013).

[4] L. Arzamasskiy, M. W. Kunz, J. Squire, E. Quataert, and A. A. Schekochihin, Kinetic turbulence in collisionless high-β plasmas, Phys. Rev. X **13**, 021014 (2023).

[5] S. D. Bale, J. C. Kasper, G. G. Howes, E. Quataert, C. Salem, and D. Sundkvist, Magnetic fluctuation power near proton temperature anisotropy instability thresholds in the solar wind, Phys. Rev. Lett. **103**, 211101 (2009).

[6] D. Verscharen, B. D. G. Chandran, K. G. Klein, and E. Quataert, Collisionless isotropization of the solar-wind protons by compressive fluctuations and plasma instabilities, Astrophys. J. **831**, 128 (2016).

[7] P. H. Yoon, Kinetic instabilities in the solar wind driven by temperature anisotropies, Rev. Mod. Plasma Phys. **1**, 4 (2017).

[8] P. H. Yoon, M. Lazar, C. Salem, J. Seough, M. M. Martinović, K. G. Klein, and R. A. López, Boundary of the distribution of solar wind proton beta versus temperature anisotropy, Astrophys. J. **969**, 77 (2024).

[9] B. A. Maruca, R. A. Qudsi, B. L. Alterman, B. M. Walsh, K. E. Korreck, D. Verscharen, R. Bandyopadhyay, R. Chhiber, A. Chasapis, T. N. Parashar, W. H. Matthaeus, and M. L. Goldstein, The trans-heliospheric survey. Radial trends in plasma parameters across the heliosphere, Astron. Astrophys. **675**, A196 (2023).

[10] Yogesh *et al.*, Solar wind heating near the sun: A radial evolution approach, Astrophys. J. **999**, 225 (2026).

[11] S. Vafin, M. Riazantseva, and M. Pohl, Coulomb collisions as a candidate for temperature anisotropy constraints in the solar wind, Astrophys. J. Lett. **871**, L11 (2019).

[12] N. J. Fox, M. C. Velli, S. D. Bale, R. Decker, A. Driesman, R. A. Howard, J. C. Kasper, J. Kinnison, M. Kusterer, D. Lario, M. K. Lockwood, D. J. McComas, N. E. Raouafi, and A. Szabo, The solar probe plus mission: Humanity's first visit to our star, Space Sci. Rev. **204**, 7 (2016).

[13] J. C. Kasper *et al.*, Parker Solar Probe enters the magnetically dominated solar corona, Phys. Rev. Lett. **127**, 255101 (2021).

[14] N. Meyer-Vernet, *Basics of the Solar Wind* (Cambridge University Press, Cambridge, England, 2007).

[15] J. C. Kasper and K. G. Klein, Strong preferential ion heating is limited to within the solar Alfvén surface, Astrophys. J. **877**, L35 (2019).

[16] B. D. G. Chandran, B. Li, B. N. Rogers, E. Quataert, and K. Germaschewski, Perpendicular ion heating by low-frequency Alfvén-wave turbulence in the solar wind, Astrophys. J. **720**, 503 (2010).

[17] M. M. Martinović *et al.*, The enhancement of proton stochastic heating in the near-sun solar wind, Astrophys. J. Suppl. Ser. **246**, 30 (2020).

[18] J. V. Hollweg, Potential wells, the cyclotron resonance, and ion heating in coronal holes, J. Geophys. Res. **104**, 505 (1999).

[19] S. R. Cranmer, Ion cyclotron wave dissipation in the solar corona: The summed effect of more than 2000 ion species, Astrophys. J. **532**, 1197 (2000).

[20] T. A. Bowen, I. Y. Vasko, S. D. Bale, Benjamin D. G. Chandran, A. Chasapis, T. Dudok de Wit, A. Mallet, M. McManus, R. Meyrand, M. Pulupa, and J. Squire, Extended cyclotron resonant heating of the turbulent solar wind, Astrophys. J. **972**, L8 (2024).

[21] T. A. Bowen, T. Ervin, A. Mallet, B. D. G. Chandran, N. Sioulas, P. A. Isenberg, S. D. Bale, J. Squire, K. G. Klein, and O. Pezzi, Stochastic heating in the sub-Alfvénic solar wind, Phys. Rev. Lett. **135**, 255201 (2025).

[22] S. Adhikari, R. Bandyopadhyay, J. Goodwill, W. H. Matthaeus, D. Ruffolo, P. Thepthong, P. Pongkitiwanichakul, S. Roy, F. Pecora, R. Chhiber, R. Pradata, A. Usmanov, M. Stevens, S. Badman, O. Romeo, J. Wang, and M. L. Goldstein, Characterization of the Alfvén transition in the young solar wind using Parker Solar Probe observations approaching solar maximum, Astrophys. J. **997**, 259 (2026).

[23] L. Matteini, S. Landi, P. Hellinger, F. Pantellini, M. Maksimovic, M. Velli, B. E. Goldstein, and E. Marsch, Evolution of the solar wind proton temperature anisotropy from 0.3 to 2.5 A.U., Geophys. Res. Lett. **34**, L20105 (2007).

[24] T. Ďurovcová, J. Šafránková, and Z. Němeček, Evolution of relative drifts in the expanding solar wind: Helios observations, Sol. Phys. **294**, 97 (2019).

[25] C. H. K. Chen, L. Matteini, A. A. Schekochihin, M. L. Stevens, C. S. Salem, B. A. Maruca, M. W. Kunz, and S. D. Bale, Multi-species measurements of the firehose and mirror instability thresholds in the solar wind, Astrophys. J. Lett. **825**, L26 (2016).

[26] K. G. Klein, B. L. Alterman, M. L. Stevens, D. Vech, and J. C. Kasper, Majority of solar wind intervals support ion-driven instabilities, Phys. Rev. Lett. **120**, 205102 (2018).

[27] M. M. Martinović and K. G. Klein, Ion-driven instabilities in the inner heliosphere. II. Classification and multidimensional mapping, Astrophys. J. **952**, 14 (2023).
[28] T. H. Stix, *Waves in Plasmas* (Springer, New York, 1992).
[29] S. P. Gary, *Theory of Space Plasma Microinstabilities* (Cambridge University Press, Cambridge, England, 1993).
[30] J. C. Kasper, A. J. Lazarus, and S. P. Gary, Wind/SWE observations of firehose constraint on solar wind proton temperature anisotropy, Geophys. Res. Lett. **29**, 1839 (2002).
[31] J. Huang *et al.*, Proton temperature anisotropy variations in inner heliosphere estimated with the first Parker Solar Probe observations, Astrophys. J. Suppl. Ser. **246**, 70 (2020).
[32] M. M. Martinović, K. G. Klein, T. Ďurovcová, and B. L. Alterman, Ion-driven instabilities in the inner heliosphere. I. Statistical trends, Astrophys. J. **923**, 116 (2021).
[33] R. Bandyopadhyay, R. A. Qudsi, S. P. Gary, W. H. Matthaeus, T. N. Parashar, B. A. Maruca, V. Roytershteyn, A. Chasapis, B. L. Giles, D. J. Gershman, C. J. Pollock, C. T. Russell, R. J. Strangeway, R. B. Torbert, T. E. Moore, and J. L. Burch, Interplay of turbulence and proton-microinstability growth in space plasmas, Phys. Plasmas **29**, 102107 (2022).
[34] Y. Tong, I. Y. Vasko, A. V. Artemyev, S. D. Bale, and F. S. Mozer, Statistical study of whistler waves in the solar wind at 1 A.U., Astrophys. J. **878**, 41 (2019).
[35] D. Verscharen, B. D. G. Chandran, E. Boella, J. Halekas, M. E. Innocenti, V. K. Jagarlamudi, A. Micera, V. Pierrard, Š. Štverák, I. Y. Vasko, M. Velli, and P. L. Whittlesey, Electron-driven instabilities in the solar wind, Front. Astron. Space Sci. **9**, 951628 (2022).
[36] J. H. Wang, T. S. Horbury, L. Matteini, and D. Trotta, Alpha-proton relative drift: Implications for the origins and dynamics of the solar wind, Astrophys. J. Lett. **978**, L17 (2025).
[37] W. Daughton and S. P. Gary, Electromagnetic proton/proton instabilities in the solar wind, J. Geophys. Res. **103**, 20613 (1998).
[38] W. Daughton, S. P. Gary, and D. Winske, Electromagnetic proton/proton instabilities in the solar wind: Simulations, J. Geophys. Res. **104**, 4657 (1999).
[39] P. Hellinger and P. M. Trávníček, Protons and alpha particles in the expanding solar wind: Hybrid simulations, J. Geophys. Res. Space Phys. **118**, 5421 (2013).
[40] K. G. Klein and G. G. Howes, Predicted impacts of proton temperature anisotropy on solar wind turbulence, Phys. Plasmas **22**, 032903 (2015).
[41] K. G. Klein, J. C. Kasper, K. E. Korreck, and M. L. Stevens, Applying Nyquist's method for stability determination to solar wind observations, J. Geophys. Res. Space Phys. **122**, 9815 (2017).
[42] K. G. Klein, G. G. Howes, and C. R. Brown, PLUME: Plasma in a linear uniform magnetized environment, Res. Notes AAS **9**, 102 (2025).
[43] D. Verscharen, K. G. Klein, B. D. G. Chandran, M. L. Stevens, C. S. Salem, and S. D. Bale, ALPS: The arbitrary linear plasma solver, J. Plasma Phys. **84**, 905840403 (2018).
[44] K. G. Klein and D. Verscharen, The dielectric response of plasmas with arbitrary gyrotropic velocity distributions, Phys. Plasmas **32**, 092104 (2025).
[45] See Supplemental Material at http://link.aps.org/supplemental/10.1103/nlq9-2g37 for the details of the simulation codes and dispersion solver software used. It also covers higher resolution description of the simulation results shown in the main article, which includes Refs. [46–49].
[46] K. G. Klein, M. Martinović, D. Stansby, and T. S. Horbury, Linear stability in the inner heliosphere: Helios re-evaluated, Astrophys. J. **887**, 234 (2019).
[47] L. Ofman and M. Gedalin, Two-dimensional hybrid simulations of quasi-perpendicular collisionless shock dynamics: Gyrating downstream ion distributions, J. Geophys. Res. Space Phys. **118**, 1828 (2013).
[48] L. Ofman, A. F. Viñas, and Y. Maneva, Two-dimensional hybrid models of H^{+}-He^{++} expanding solar wind plasma heating, J. Geophys. Res. Space Phys. **119**, 4223 (2014).
[49] D. Verscharen, S. Bourouaine, and B. D. G. Chandran, Instabilities driven by the drift and temperature anisotropy of alpha particles in the solar wind, Astrophys. J. **773**, 163 (2013).
[50] C. F. Kennel and F. Engelmann, Velocity space diffusion from weak plasma turbulence in a magnetic field, Phys. Fluids **9**, 2377 (1966).
[51] D. Verscharen, S. Bourouaine, B. D. G. Chand ran, and B. A. Maruca, A parallel-propagating Alfvénic ion-beam instability in the high-beta solar wind, Astrophys. J. **773**, 8 (2013).
[52] R. Huang, G. G. Howes, and A. J. McCubbin, The velocity-space signature of transit-time damping, J. Plasma Phys. **90**, 535900401 (2024).
[53] K. G. Klein, D. Larson, R. Livi, A. Martinovic, M. M. and Rahmati, N. Shankarappa, M. Stevens, D. Verscharen, and P. Whittlesey, Ion-scale wave emission and absorption for non-Maxwellian velocity distributions in the inner heliosphere, Geophys. Res. Lett. **53**, 118809 (2026).
[54] B. L. Alterman, The significance of proton beams in the multiscale solar wind, Ph.D. thesis, University of Michigan, 2019.
[55] J. L. Verniero *et al.*, Parker Solar Probe observations of proton beams simultaneous with ion-scale waves, Astrophys. J. Suppl. Ser. **248**, 5 (2020).
[56] B. Short, D. M. Malaspina, A. Chasapis, and J. L. Verniero, Quiescent solar wind regions in the near-sun environment: Properties and radial evolution, Astrophys. J. Lett. **975**, 218 (2024).
[57] L. Ofman and A. F. ViñAs, Two-dimensional hybrid model of wave and beam heating of multi-ion solar wind plasma, J. Geophys. Res. Space Phys. **112**, A06104 (2007).
[58] L. Ofman, Hybrid model of inhomogeneous solar wind plasma heating by Alfvén wave spectrum: Parametric studies, J. Geophys. Res. Space Phys. **115**, A04108 (2010).
[59] L. Ofman, A. Koval, L. B. Wilson, and A. Szabo, Understanding the role of α particles in oblique heliospheric shock oscillations, J. Geophys. Res. Space Phys. **124**, 2393 (2019).
[60] L. Ofman, S. A. Boardsen, L. K. Jian, J. L. Verniero, and D. Larson, Modeling ion beams, kinetic instabilities, and waves observed by the Parker Solar Probe near perihelia, Astrophys. J. **926**, 185 (2022).
[61] L. Ofman, S. A. Boardsen, L. K. Jian, P. Mostafavi, J. L. Verniero, R. Livi, M. McManus, A. Rahmati, D. Larson, and M. L. Stevens, Observations and modeling of unstable

proton and α particle velocity distributions in sub-Alfvénic solar wind at Parker Solar Probe perihelia, Astrophys. J. **954**, 109 (2023).

[62] L. Ofman, Yogesh, S. A. Boardsen, P. Mostafavi, L. K. Jian, V. M. Sadykov, K. Klein, and M. Martinovic, Modeling hot, anisotropic ion beams in the solar wind motivated by the Parker Solar Probe observations near perihelia, Astrophys. J. **984**, 174 (2025).

[63] D. Winske and N. Omidi, *Computer Space Plasma Physics: Simulation Techniques and Software*, edited by H. Matsumoto and Y. Omura (Terra SP, Tokyo, 1993), pp. 103–160.

[64] Yogesh, L. Ofman, S. A. Boardsen, K. Klein, M. Martinovic, V. M. Sadykov, J. Verniero, N. Shankarappa, L. K. Jian, P. Mostafavi, J. Huang, and K. W. Paulson, Evidence of interaction between ion-scale waves and ion velocity distributions in the solar wind, arXiv:2505.02999.

[65] A. Wambecq, Rational Runge-Kutta for solving systems of ordinary differential equations, Computing **20**, 333 (1978).

[66] L. Ofman and M. Gedalin, Two-dimensional hybrid simulations of quasi-perpendicular collisionless shock dynamics: Gyrating downstream ion distributions, J. Geophys. Res. Space Phys. **118**, 1828 (2013).

[67] B. J. Vasquez, Heating rate scaling of turbulence in the proton kinetic regime, Astrophys. J. **806**, 33 (2015).

[68] L. Ofman, Nonlinear evolution of ion kinetic instabilities in the solar wind, Sol. Phys. **294**, 51 (2019).

[69] L. Ofman, A. F. Viñas, and D. A. Roberts, The effects of inhomogeneous proton-α drifts on the heating of the solar wind, J. Geophys. Res. Space Phys. **122**, 5839 (2017).

[70] H. Xie, L. Ofman, and A. Viñas, Multiple ions resonant heating and acceleration by Alfvén/cyclotron fluctuations in the corona and the solar wind, J. Geophys. Res. Space Phys. **109**, A010501 (2004).

[71] S. D. Bale *et al.*, The FIELDS instrument suite for solar probe plus. Measuring the coronal plasma and magnetic field, plasma waves and turbulence, and radio signatures of solar transients, Space Sci. Rev. **204**, 49 (2016).

[72] M. D. McManus, K. G. Klein, S. D. Bale, T. A. Bowen, J. Huang, D. Larson, R. Livi, A. Rahmati, O. Romeo, J. Verniero, and P. Whittlesey, Proton- and alpha-driven instabilities in an ion cyclotron wave event, Astrophys. J. **961**, 142 (2024).

[73] M. M. Martinović, K. G. Klein, R. De Marco, D. Verscharen, R. D'Amicis, and R. Bruno, Impact of two-population α-particle distributions on plasma stability, Astrophys. J. Lett. **988**, L25 (2025).